(Received 5 September 2025, Accepted 15 October 2025, Scheduled 24 October 2025)

Circularly Polarized Holographic Metasurface Antenna with Metal Vias and Its Gain Enhancement Analysis

Chunyu Liu[1], Chen Zhang[1,*], Xuwen Guo[1], and Huayong Zou[2]

[1] *School of Electronic Engineering, Tianjin University of Technology and Education, Tianjin 300222, China*
[2] *Tianjin 712 Mobile Communications Co., Ltd, Tian Jin 300222, China*

ABSTRACT: This paper presents a design method for circularly polarized metasurface antennas by integrating waveguide-fed metasurfaces with optical holography principles. Two interleaved linear slot elements on the metasurface top layer are excited by a reference wave from the feed, generating a circularly polarized beam. Simply adjusting the position of each slot element steers the beam in the desired direction. To enhance gain, metal vias are added around the antenna perimeter, reducing reference wave leakage. To validate this method, two 24 GHz circularly polarized holographic metasurfaces were simulated and experimentally characterized. Measurements show a 1.23 dB gain enhancement in the metasurface antenna with metal vias. Simulated and measured results validate the antenna's performance. This approach yields compact, low-profile antennas without requiring a separate feed network. Furthermore, the structure can be extended to create reconfigurable circularly polarized antennas, demonstrating significant potential in this field.

1. INTRODUCTION

As modern communications advance, linearly polarized antennas require precise positioning. Minor misalignment can significantly reduce the efficiency of receiving antenna, adversely impacting overall system performance. Conversely, circularly polarized (CP) antennas — with only left- or right-handed polarization —– are immune to spatial orientation. Consequently, CP antennas are increasingly replacing linear ones in modern systems to avoid polarization mismatch. Current research focuses on developing feed techniques for high-purity CP antennas. However, these techniques often result in antennas with high profiles and large sizes [1]. Reducing antenna profile and size therefore remains a critical research challenge.

Metasurfaces are artificial structures composed of subwavelength unit cells arranged periodically or non-periodically. Due to their low profile and ease of integration, metasurfaces have been applied to antenna design, leading to metasurface antennas. The research into metasurfaces with high impedance characteristics led Sievenpiper et al. to first propose combining impedance modulation theory with holographic principles, establishing holographic impedance modulation surfaces [2]. Thus, holographic metasurface antennas became a major research focus. The core concept relies on the holographic principle from physical optics. It involves creating the required holographic surface pattern through the interference between a reference wave and a desired target wave. Illuminating this surface with the reference wave then reconstructs the target wave. The structure is remarkably simple, requiring only a feed source and holographic surface. Recent advances in holographic metasurface technology have made beam synthesis a significant research focus [3–5]. Cui's group extended their research on holographic metasurface antennas to multi-frequency multi-beam operation, beam synthesis, and linear-to-circular polarization conversion [6–8]. This approach eliminates complex feed networks while enabling simpler, lower-cost fabrication. To address the issues of high profile and large size in conventional circularly polarized antennas, holographic metasurface technology was chosen to achieve antenna miniaturization and circular polarization [9–13].

However, in conventional holographic impedance-modulation surfaces, the surface elements are permanently fixed upon fabrication, which rigidly defines their functionality and renders dynamic control exceedingly challenging. To address this, Smith's team proposed a method combining polarized particles with holographic metasurfaces [14]. This approach enables control over the state of each unit cell, creating a digitally controllable, dynamically reconfigurable holographic metasurface antenna. Using this method, the team later demonstrated dual-linear polarization operation [15]. Subsequently, Deng's team employed the same principle to develop a holographic metasurface antenna generating a circularly polarized beam [16], and later extended it to produce circularly polarized quasi-non-diffracting vortex waves carrying orbital angular momentum (OAM) [17]. Sleasman's team experimentally demonstrated multiple complex radiation patterns through dynamic coding of surface unit cells. This validates the potential of their diode-controlled digital metasurface architecture for microwave imaging systems [18]. Hoang et al. proposed a novel unit structure integrating Jerusalem cross patches into crossed-slot elements to investigate polarization imaging in metasurface antennas [19]. Most of the existing metasurface technologies involve impedance modulation,

* Corresponding author: Chen Zhang (2021110004@tute.edu.cn).

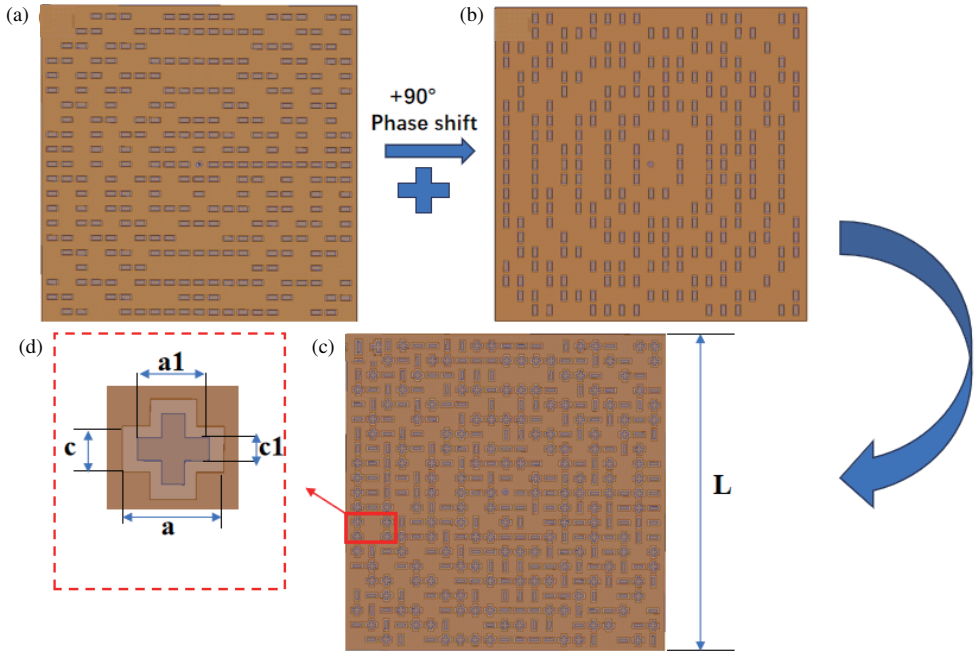

FIGURE 1. Principle of circular polarization generation. (a) Y-polarized holographic metasurface antenna model. (b) X-polarized holographic metasurface antenna model. (c) Circular polarizd holographic metasurface antenna model. (d) Metasurface unit model.

designing metasurfaces by extracting the surface impedance of the unit. The proposed antenna in this paper is a new type of holographic metasurface antenna. This metasurface antenna has elements different from impedance-modulated surfaces and the potential for reconfigurable metasurface development. By processing its surface elements, the concept of reconfigurability can be realized, which is more conducive to practical applications than continuous impedance-modulated antennas. For holographic metasurface antennas based on polarized particles, the unit cell design offers greater flexibility. Consequently, metasurface unit design has become a key research focus. Modifying the unit cell structure enhances antenna performance and facilitates future reconfigurable designs. Furthermore, the design concept of our holographic metasurface antenna shares significant commonality with emerging metasurface-based sensors [20]. Both rely on the precise control of unit cell responses. The single-substrate, low-cost design principle emphasized in sensing work provides a valuable direction for our future antenna optimization. This synergy underscores the potential of metasurfaces as a versatile platform for high-performance RF systems.

High gain remains a key focus in antenna research. For the proposed holographic metasurface antenna generating circularly polarized beams, improving its gain is an important next step. To address this problem, recent methods often integrate metal vias into antennas to enhance performance. Significant progress has been made in areas like gain and radiation efficiency improvement [21, 22] and beam steering [23]. Therefore, we propose a holographic metasurface antenna loading with metal vias worked at 24 GHz. This method suppresses energy leakage, effectively enhancing the gain of the circularly polarized metasurface antenna.

This paper presents a novel holographic metasurface antenna by integrating the holographic principle with polarization particles. Unlike traditional phased arrays, it requires no complex feed network, phase shifters, or external feeds. It offers higher efficiency by coupling guided waves via slots, enables reconfigurability through impedance modulation, and features a compact, low profile, showing great potential to replace phased arrays in miniaturized applications.

2. PRINCIPLE AND ANALYSIS

Achieving circular polarization requires equal amplitude and a 90° phase difference between the horizontal and vertical electric field components, as illustrated in Fig. 1. To meet this requirement, we propose a metasurface design incorporating transverse and longitudinal slots. The transverse slots couple the x-component of the reference wave magnetic field, while the longitudinal slots couple the y-component, effectively creating two linearly polarized reference beams. A 90° phase difference is introduced into the target wave equations for these two beams. This generates distinct slot arrangement patterns for each polarization, where transverse and longitudinal slots overlap, and they form a cross-slot structure. This design enables the generation of two orthogonal linear polarizations with equal amplitude and a 90° phase difference on a single metasurface. They combine to produce a circularly polarized beam. Additionally, metal patches are added within the slots to enhance radiation intensity. As shown in Fig. 2, to increase antenna gain, metal vias are placed around the antenna perimeter. This reduces energy leakage from the holographic metasurface, achieving the desired gain improvement.

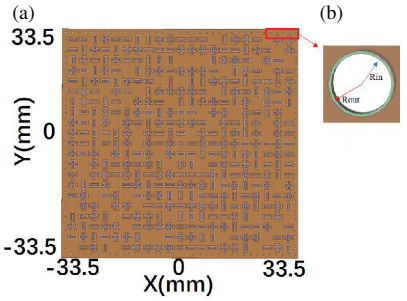

FIGURE 2. Model of the metasurface antenna with metal vias. (a) Circularly polarized metasurface antenna with loaded metal vias. (b) Metal vias model.

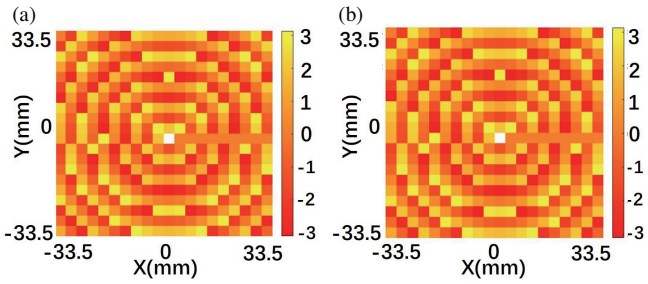

FIGURE 3. Phase distribution of the 24 GHz reference wave. (a) The x-component (Hx). (b) The y-component (Hy).

Based on the described principles and unit structure, a 24-GHz circularly polarized metasurface antenna comprising 21×21 unit cells was designed. The antenna features a three-layer parallel-plate waveguide structure. The middle layer is a Rogers 3003 substrate ($\varepsilon_r = 3$, $\tan\delta = 0.001$, height $h1 = 1.542$ mm). Rogers 3003 was selected as the substrate for two reasons. First, its consistent permittivity, crucial for maintaining the precise geometry of metasurface units, prevents resonant frequency shifts and performance degradation. Second, its low loss tangent contributes to higher antenna gain. The top and ground layers of the metasurface antenna are fabricated on a single copper-clad substrate. The top conductor is etched with slot units, leaving no gap between layers to adversely affect the gain or impedance matching. A coaxial feed, centrally inserted through the bottom plate, provides excitation. The top copper plate is discretized into an array of unit cells. The metasurface antenna unit cell, illustrated in Fig. 1(d), features a slot and metal patch with dimensions $a = 2.63$ mm, $c = 1.2$ mm, $a1 = 1.85$ mm, and $c1 = 0.6$ mm. Each unit cell is 3.125 mm long, and dimensions of the metasurface unit and its slot were determined through parametric optimization. The final unit length was optimized to $\lambda/4$. The full antenna comprises a 21×21 array of these unit cells. For the design with metal vias (Fig. 2(b)), each via consists of a cylinder with outer radius $Rout = 0.22$ mm and inner radius $Rin = 0.2$ mm. The via diameter was carefully optimized. A small diameter reduces radiation efficiency and gain, while a larger one offers diminishing returns and faces fabrication limits. The final diameter was chosen accordingly.

A monopole feed embedded at the antenna center generates the reference wave for coupling to the metasurface slot elements. Thus, the reference wave can be described by the zeroth-order Hankel function of the first kind:

$$H_{ref} = \begin{cases} H_0^{(1)}(k_g r)\sin(\phi), & H_x \\ H_0^{(1)}(k_g r)\cos(\phi), & H_y \end{cases} \quad (1)$$

Here, k_g represents the wavenumber in the substrate, r the distance from a discrete aperture location on the top layer to the central origin, and ϕ the azimuth angle at each point on the metasurface antenna. The phase distributions for the different reference wave components were then calculated using MATLAB software, as shown in Fig. 3.

The radiation principle of holographic metasurface antennas shows that coupling the reference wave with the designed metasurface unit cells generates a beam in the desired direction. To achieve this target, phase compensation is applied to the coaxial-port-excited reference wave using the designed metasurface. This compensation converts the reference wave field distribution H at all discrete element locations into the desired target beam field distribution P. The required holographic phase pattern and slot distribution are then calculated from H and P.

When being illuminated by the reference wave, each discrete slot element position on the metasurface possesses a specific phase value. To determine if a slot should be etched at a position, a phase difference threshold is compared. If the phase difference at a position is below this threshold, phase compensation is required, and a slot is etched. This etched slot couples energy effectively and radiates. Conversely, if the phase difference exceeds the threshold, no compensation is needed, the slot not etched, and the position remains non-radiating.

The selection of the threshold in holographic metasurface antennas is critical, as it directly determines the number of etched slots. Selecting a higher threshold increases the number of units meeting the etching condition. This increases the number of radiating elements and improves radiation intensity. However, an excessively high threshold results in too many radiate units, introducing significant interference, increasing beam side lobes, and degrading directivity. Therefore, the threshold must be chosen to maximize radiation intensity while maintaining good directivity. Based on this trade-off, the designed holographic metasurface antenna in this work uses a phase threshold of 120° to achieve optimal radiation performance.

To achieve correct phase compensation, we first derive the field distribution P of the target wave at the metasurface unit position to calculate the phase difference. The phase difference ϕ_r is expressed using the following Equaiton (2):

$$\phi_r(x,y) = \phi_{r_0}(x,y) - k_0 \sin\theta_r \left[x\cos(\varphi_r) + y\sin(\varphi_r)\right] \quad (2)$$

Here, θr and φr are the elevation and azimuth angles of the radiation beam, respectively. ϕ_{r_0} denotes the initial phase of the target wave. θr and φr determine the target wave's radiation direction; coordinates (x, y) denote the position of metasurface unit cells. This work aims to generate a linearly polarized target wave via the formula, then superimpose it with an equal-amplitude 90°-phase-shifted version to form the desired circularly polarized beam. This CP beam is defined as the tar-

get wave P_{obj}, and its field distribution is given by Equation (3):

$$P_{obj} = e^{-j\phi_r(x,y)} = e^{-j\{\phi_{r_0}(x,y) - k_0 \sin\theta_r[x\cos(\varphi_r)+y\sin(\varphi_r)]\}} \quad (3)$$

The holographic metasurface antenna functions as an interference pattern defined by the reference and target fields, expressed in Equation (4). My and Mx represent the y-polarized and x-polarized interferograms.

$$M_y = P_{objy}H^*_{refx}; M_x = P_{objx}H^*_{refy} \quad (4)$$

where H^*_{refx} and H^*_{refy} are the complex conjugate of the reference magnetic field. As shown in Fig. 4, the unit distributions on the metasurface can be calculated by Equation (4). They correspond to the horizontal (Mx) and vertical (My) magnetic apertures. Comparing these distributions with the threshold yields three radiation patterns: horizontal slots coupling the x-component, vertical slots coupling the y-component, and cross-shaped slots coupling both components. Based on a hologram calculated from a predefined target beam, the metasurface is implemented with unit cells chosen from three types: horizontal, vertical, or cross-shaped slots. The final radiation pattern distribution (Ma), given by $Ma = Mx + My$, is shown in Fig. 5. This distribution data enables the modeling and simulation of the metasurface antenna.

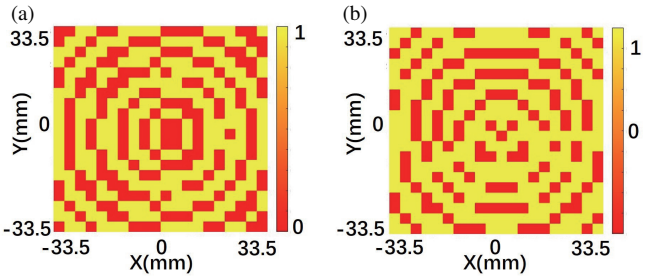

FIGURE 4. Slot distribution of the proposed metasurface unit cells. (a) The horizontal slots (Mx). (b) The vertical slots (My).

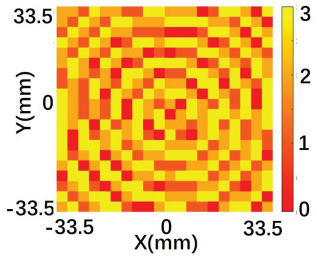

FIGURE 5. The final distribution pattern (Ma) of elements on the designed CP metasurface.

3. EXPERIMENT AND VERIFICATION

To verify the proposed method and demonstrate the gain advantage of metasurfaces with metallic vias, two circularly polarized metasurfaces operating at 24 GHz were designed and fabricated. The fabricated CP metausrface and another prototype with metal vias are shown in Fig. 6(a), respectively. Measurement setup of the metasurfaces is illustrated in Fig. 6(b). The operating frequency of this circularly polarized holographic metasurface antenna is 23.5–-24.5 GHz. The measurement setup is as follows. First, a horn antenna for the target band is mounted on a polarization positioner. Second, as shown in Fig. 6(b), the antenna under test is fixed on the test bench and directly fed with power through the cable. Then, the test bench rotates 360 degrees horizontally. At the same time, the transmitting antenna, placed according to the polarization position, will also rotate. The received power is recorded during rotation to obtain the far-field radiation characteristics.

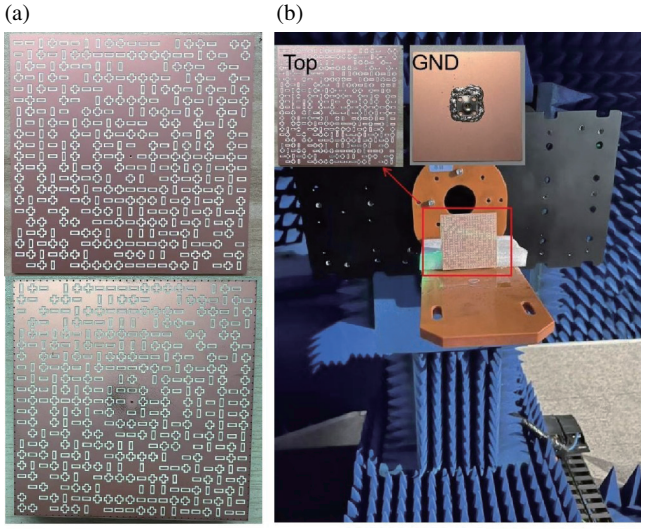

FIGURE 6. Fabricated prototype and measurement setup for CP metasurface antenna. (a) Prototypes with and without metallic vias. (b) Measurement setup.

As shown in Fig. 7, the measured reflection coefficient (S_{11}) of both fabricated metasurface antennas remains below -10 dB across 23.5–24.5 GHz, demonstrating good impedance matching. Fig. 7 compares the simulated and measured S_{11}. The curves show discrepancies. First, minor fabrication errors in the small slots cause a slight resonant frequency shift. Second, dimensional inaccuracies during monopole cutting and welding shift the overall response. Nevertheless, the measured results agree with the simulation in overall trend and performance.

In circularly polarized antennas, axial ratio (AR) quantifies the purity of the circular polarization. An AR below 3 dB generally indicates good circular polarization. Fig. 8 shows the measured AR of the metasurface antenna. A bandwidth of 0.25 GHz with AR below 3 dB is achieved, demonstrating the antenna's ability to radiate circularly polarized waves. AR bandwidth of the metasurface is narrow; however, this problem can be solved by using other advanced units in future. Fig. 8 shows a discrepancy between the measured and simulated ARs. This is likely due to misalignment between the transmitting and receiving antennas, as precise boresight alignment is critical for accurate AR measurement, especially with narrow beamwidth antennas. Despite this, the measured results remain within a reasonable range.

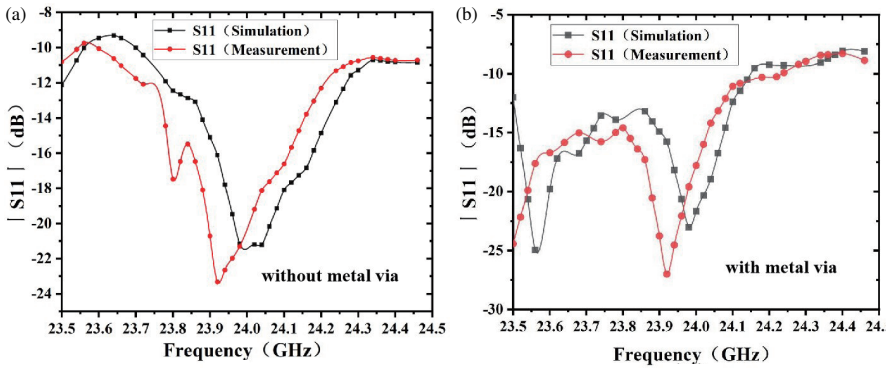

FIGURE 7. The simulated and measured reffection coefffcients of two kinds of 24 GHz CP metasurfaces. (a) Reflection coefficients of the metasurface antenna without metal vias. (b) Reflection coefficients of the metasurface antenna with metal vias.

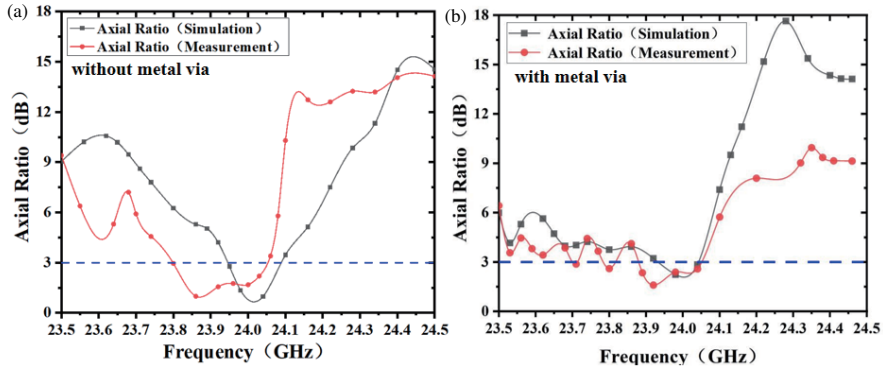

FIGURE 8. The simulated and measured axial ratios of two kinds of 24 GHz CP metasurfaces. (a) Axial ratio of the metasurface antenna without metal vias. (b) Axial ratio of the metasurface antenna with metal vias.

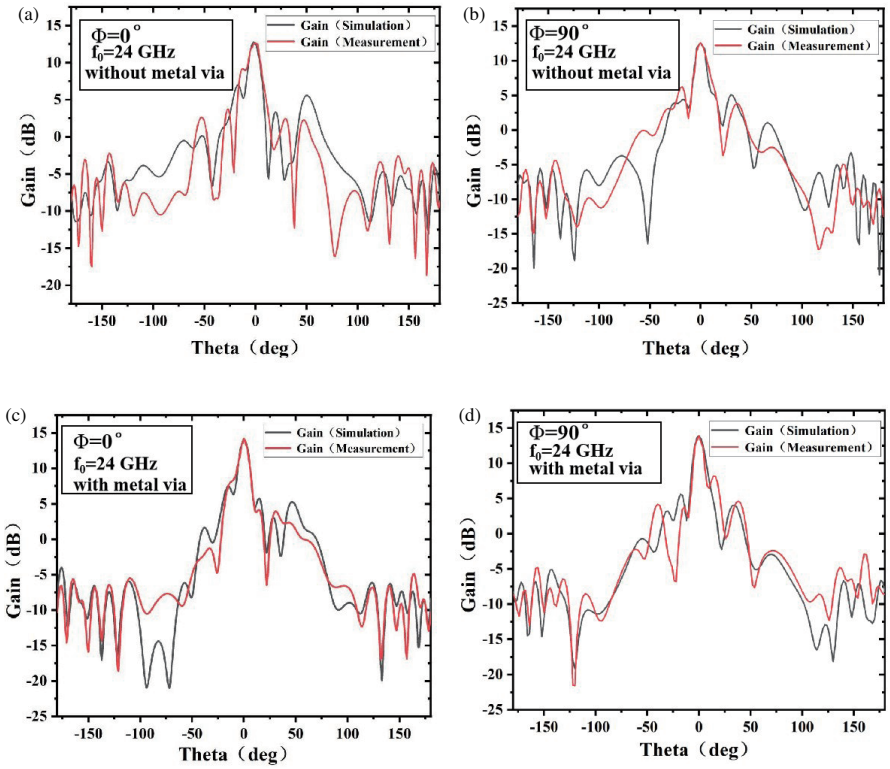

FIGURE 9. The simulated and measured far-field radiation patterns of two kinds of 24 GHz CP metasurfaces. (a), (b) Far-field radiation patterns of the metasurface antenna without metal vias. (c), (d) Far-field radiation patterns of the metasurface antenna with metal vias. ($\phi = 0°$ and $\phi = 90°$ cuts.

Figure 9 shows the measured total gain of the two circularly polarized holographic metasurface antennas at $\phi = 0°$ and $\phi = 90°$. The plots confirm the desired circularly polarized beam radiating along the normal direction. The range of the first side lobe of the metasurface antenna is 6 dB to 8 dB. The side lobe is relatively large, which might be due to the large number of elements. While the overall measured gain response differs slightly from the simulation due to fabrication and testing tolerances, the maximum gain remains in good agreement. Crucially, Figs. 9(a) and 9(c) show that the antenna without metal vias achieves a peak gain of 12.76 dB, while the antenna with metal vias reaches 13.98 dB, with gain enhancement of 1.23 dB. These measurement results validate the effectiveness of adding metal vias around the antenna perimeter to increase gain.

4. CONCLUSION

This study presents a novel unit cell design for holographic metasurface antennas generating circularly polarized beams using surface wave excitation worked in 24 GHz. To increase antenna gain and reduce energy leakage, metal vias were added around the metasurface perimeter, reducing energy leakage. Simulations, fabrication, and measurements validated this approach. Further gain enhancement for this metasurface remains possible by optimizing the via position and size. However, our experiments did not reveal a clear trend, indicating that more extensive investigation is required to explore the performance limits of this method. The simple structure was maintained while improving gain, preserving the antenna's low-profile, compact, and easily integrable advantages. The proposed circularly polarized metasurface antenna, based on the polarization particle method, features tunable polarization and radiation patterns. The agreement between simulation and measurement confirms its ability to generate a CP beam in any direction within the upper hemisphere, offering a new approach to CP antenna design. Furthermore, this novel unit cell offers a pathway for developing reconfigurable high-gain antennas.

ACKNOWLEDGEMENT

This work was supported by the Tianjin Education Commission Research Program Project under Grant 2023KJ191.

REFERENCES

[1] Nikoufard, M., A. Nourmohammadi, and S. Esmaeili, "Hybrid plasmonic nanoantenna with the capability of monolithic integration with laser and photodetector on InP substrate," *IEEE Transactions on Antennas and Propagation*, Vol. 66, No. 1, 3–8, 2018.

[2] Sievenpiper, D., J. Colburn, B. Fong, J. Ottusch, and J. Visher, "Holographic artificial impedance surfaces for conformal antennas," in *2005 IEEE Antennas and Propagation Society International Symposium*, Vol. 1B, 256–259, Washington, DC, USA, 2005.

[3] Huang, H.-F. and Y.-J. Ma, "Generation of dual-band dual-polarized orbital angular momentum beams with holographic impedance metasurface," in *2023 IEEE MTT-S International Wireless Symposium (IWS)*, 1–3, Qingdao, China, 2023.

[4] Zhao, S., S. Zhang, H. Xue, Y. Li, K. Zhang, H. Liu, and L. Li, "Generation of bessel beam with controllable circular polarization and direction using Holographic Tensor Metasurface," *IEEE Antennas and Wireless Propagation Letters*, Vol. 23, No. 3, 985–989, 2024.

[5] Huang, H. and Y. Ma, "Tensor holographic impedance coding metasurface for millimeter-wave circular airy OAM multibeams generation," in *2024 IEEE International Workshop on Radio Frequency and Antenna Technologies (iWRF&AT)*, 389–394, Shenzhen, China, 2024.

[6] Wang, J., J. Lou, J. F. Wang, S. B. Qu, H. L. Du, and T. J. Cui, "Ferroelectric composite artificially-structured functional material: Multifield control for tunable functional devices," *Journal of Physics D: Applied Physics*, Vol. 55, No. 30, 303002, 2022.

[7] Liu, C., Q. Ma, Z. J. Luo, Q. R. Hong, Q. Xiao, H. C. Zhang, L. Miao, W. M. Yu, Q. Cheng, L. Li, and T. J. Cui, "A programmable diffractive deep neural network based on a digital-coding metasurface array," *Nature Electronics*, Vol. 5, No. 2, 113–122, 2022.

[8] Yan, T., Q. Ma, and T. Cui, "Circular polarization hologram realized by pancharatnam-berry phase in microwave frequency," *Journal of Computer and Communications*, Vol. 8, No. 12, 134–141, 2020.

[9] Liang, H., Z. Jiang, S. Meng, C. Peng, and W. Gao, "A conformal CP antenna based on isotropic holographic metasurface," in *2024 Photonics & Electromagnetics Research Symposium (PIERS)*, 1–5, Chengdu, China, 2024.

[10] Purohit, G., S. Ghosh, and C. Saha, "Circular and linearly polarized high gain scalar holographic metasurface antenna for mm-wave application," in *2024 IEEE International Conference on Electronics, Computing and Communication Technologies (CONECCT)*, 1–5, Bangalore, India, 2024.

[11] Shi, T., R. Chai, X. Chen, M. Li, T. Zhang, and M.-C. Tang, "A low-profile, circularly polarized, metasurface-based antenna with enhanced bandwidth and stable high gain," *IEEE Antennas and Wireless Propagation Letters*, Vol. 22, No. 2, 253–257, 2023.

[12] Liu, J., J.-Y. Li, and Z. N. Chen, "Broadband polarization conversion metasurface for antenna RCS reduction," *IEEE Transactions on Antennas and Propagation*, Vol. 70, No. 5, 3834–3839, 2022.

[13] Pang, H., J. Zhao, and J. Xu, "Miniaturized circularly polarized metasurface antenna based on characteristic mode analysis," *Microwave and Optical Technology Letters*, Vol. 66, No. 1, e33983, 2024.

[14] Yurduseven, O., D. L. Marks, J. N. Gollub, and D. R. Smith, "Design and analysis of a reconfigurable holographic metasurface aperture for dynamic focusing in the Fresnel zone," *IEEE Access*, Vol. 5, 15 055–15 065, 2017.

[15] Yurduseven, O. and D. R. Smith, "Dual-polarization printed holographic multibeam metasurface antenna," *IEEE Antennas and Wireless Propagation Letters*, Vol. 16, 2738–2741, 2017.

[16] Zhang, C., L. Deng, J. Zhu, W. Hong, L. Wang, H. Wang, T. Zeng, X. Ren, X. He, Z. Zhao, S. Li, and X. Chen, "A right-handed circularly polarized wave generated by a waveguide-fed holographic metasurface," *Journal of Physics D: Applied Physics*, Vol. 53, No. 26, 26LT01, 2020.

[17] Zhang, C., L. Deng, L. Wang, X. Chen, and S. Li, "Generation of circularly polarized quasi-non-diffractive vortex wave via a microwave holographic metasurface integrated with a monopole," *Applied Sciences*, Vol. 11, No. 15, 7128, 2021.

[18] Sleasman, T. A., M. F. Imani, A. V. Diebold, M. Boyarsky, K. P. Trofatter, and D. R. Smith, "Implementation and characterization of a two-dimensional printed circuit dynamic metasurface aper-

ture for computational microwave imaging," *IEEE Transactions on Antennas and Propagation*, Vol. 69, No. 4, 2151–2164, 2021.

[19] Hoang, T. V., V. Fusco, T. Fromenteze, and O. Yurduseven, "Computational polarimetric imaging using two-dimensional dynamic metasurface apertures," *IEEE Open Journal of Antennas and Propagation*, Vol. 2, 488–497, 2021.

[20] Nath, U., S. Banerjee, C. Santini, R. Citroni, F. Mangini, and F. Frezza, "Simple and cost-effective design of a THz-metamaterial-based hybrid sensor on a single substrate," *Sensors*, Vol. 25, No. 12, 3660, 2025.

[21] Althuwayb, A. A., M. Alibakhshikenari, B. S. Virdee, H. Benetatos, F. Falcone, and E. Limiti, "Antenna on chip (AoC) design using metasurface and SIW technologies for THz wireless applications," *Electronics*, Vol. 10, No. 9, 1120, 2021.

[22] Alibakhshikenari, M., B. S. Virdee, R. K. Rajaguru, A. Iqbal, M. Al-Hasan, C. H. See, and F. Falcone, "High performance antenna-on-chip inspired by SIW and metasurface technologies for THz band operation," *Scientific Reports*, Vol. 13, No. 1, 56, 2023.

[23] Li, T. and Z. N. Chen, "Control of beam direction for substrate-integrated waveguide slot array antenna using metasurface," *IEEE Transactions on Antennas and Propagation*, Vol. 66, No. 6, 2862–2869, 2018.